




Microstructure analysis and quantitative strengthening evaluation of medium carbon bainitic multiphase steel

Xiaowen Sun¹, Dongyun Sun¹, Yuefeng Wang¹, Fucheng Zhang¹, Guoliang Sheng³, Yanming He³, and Tiansheng Wang^{1,2,4,*} 

¹ State Key Laboratory of Metastable Materials Science and Technology, Yanshan University, Qinhuangdao 066004, China

² National Engineering Research Center for Equipment and Technology of Cold Rolled Strip, Yanshan University, Qinhuangdao 066004, China

³ Materials Research Center, CITIC Dicastal Co. Ltd, Qinhuangdao 066004, China

⁴ Hebei Key Lab for Optimizing Metal Product Technology and Performance, Yanshan University, Qinhuangdao 066004, People's Republic of China

Received: 13 June 2022

Accepted: 30 August 2022

Published online:
19 September 2022

© The Author(s), under exclusive licence to Springer Science+Business Media, LLC, part of Springer Nature 2022

ABSTRACT

The microstructure and properties of bainitic multiphase steels with bainitic ferrite as the main phase are the focus of the current research. In the work, multiphase microstructures of pre-formed martensite (PM), bainitic ferrite (BF), and retained austenite (RA) was obtained via austempering processes in medium carbon bainitic steel. The relationship between the multiphase characteristics and mechanical properties was analyzed quantitatively. The results show that the thickness of bainitic ferrite laths and the size of blocky retained austenite of the PM-BF-RA samples are smaller than those of the BF-RA samples. The dislocation density of bainitic ferrite and carbon content in retained austenite of the PM-BF-RA samples are higher. The PM-BF-RA samples obtain higher strength. The yield strength that was calculated by measured microstructural parameters is similar to the tested value. The dominant strengthening phases of PM-BF-RA samples are pre-formed martensite and bainitic ferrite dual phases, while those of the BF-RA samples are the bainitic ferrite. The main of the strengthening mechanism of bainitic ferrite is grain boundary strengthening, while it is solid solution strengthening for martensite and retained austenite. Small and stable retained austenite with high carbon content effectively ensures the high plasticity of PM-BF-RA samples. Moreover, the high toughness of PM-BF-RA samples can be attributed to fine bainitic ferrite and small blocky retained austenite. This study demonstrates that medium carbon bainitic multiphase steel with PM-BF-RA microstructure exhibits excellent combination of strength, plasticity, and toughness.

Handling Editor: Sophie Primig.

Address correspondence to E-mail: tswang@ysu.edu.cn

Introduction

Nanobainite multiphase steel has outstanding mechanical properties and is widely applied in wear resistant steel plate, railway, and bearing [1–4]. Generally, a multiphase microstructure with pre-formed martensite, nanobainitic ferrite, and retained austenite can be obtained using a below- M_S austempering process or Q&P process [5, 6]. It is well known that the bainitic austempering process plays a crucial role in the content of the final microstructure, the microconstituents of each phase, and the morphology of the retained austenite [7, 8]. In addition, the evolution of the microstructure and the optimal microconstituents in each phase are the keys to improving the mechanical properties of multiphase steels [9, 10]. The relationship between the multiphase microstructure and the mechanical properties of samples obtained using the austempering process has been a subject of considerable attention in the recent years [11, 12].

The microstructural characteristics (phase content, size, and morphology) of bainitic ferrite and pre-formed martensite are the most important factors in multiphase microstructures, which affect the strength and hardness of the steel [13, 14]. Because of its small size and high dislocation density, bainitic ferrite lath can increase the strength and hardness of the steel [15]. It has been reported that carbides which precipitate from pre-formed martensite during the austempering process can pin dislocations and improve the yield strength [9, 16]. In addition, the size and volume fraction of bainitic ferrite and martensite/austenite (M/A) blocks decrease when the microstructure contains pre-formed martensite, but excellent comprehensive mechanical properties can still be obtained [17]. An appropriate increase in the amount of pre-formed martensite can improve the yield strength and hardness, but when the amount of pre-formed martensite exceeds 15%, the plasticity and toughness of the steel will deteriorate significantly [18]. To study the effects that multiphase microstructure has on yield strength, Navarro-López et al. established a solid solution strengthening model of carbon atoms in a multiphase system of martensite, bainitic ferrite, and retained austenite. The results showed that the phase fraction and carbon concentration are important factors that affect the yield strength. However, other microconstituents (e.g.,

dislocation and size) of the three phases are not calculated in detail [19]. In addition, it is reported in the literature that the contribution of strength was calculated on the basis of the bainite phase in a martensite/bainite mixed microstructure; however, the study ignored the calculation of phase microconstituents of martensite and retained austenite [20]. Other reports in the literature also explained the relationship between microstructure and yield strength; however, they mainly discussed a single microconstituent of different phases or different microconstituents of the same phase in the microstructure [21, 22]. Therefore, it is necessary to quantitatively study the influence of each phase and its different microconstituents on yield strength in multiphase structures.

Austenite can transform into martensite during deformation, which results in a transformation-induced plasticity (TRIP) effect that can enhance the strain hardening ability to improve plasticity and toughness [23]. Moreover, the fraction and phase microconstituents (carbon content and size) of retained austenite are related to the plasticity and toughness of martensite/bainite multiphase steel [19, 24]. Introducing pre-formed martensite in multiphase steel increases the carbon content and dislocation density of retained austenite, but it reduces the volume fraction of retained austenite that has high-carbon content, which results in a decrease in the plasticity and toughness [25]. However, Long et al. reported that the carbon content and volume fraction of retained austenite increased after the below- M_S austempering process, which exhibited excellent work hardening ability and improved plasticity-toughness [26]. Therefore, it is necessary to further study the effect that retained austenite has on the plasticity and toughness of the multiphase martensite/bainite microstructure.

In this study, pre-formed martensite, bainitic ferrite, and retained austenite multiphase microstructure was prepared using a below- M_S and above- M_S austempering process. Scanning electron microscopy (SEM), transmission electron microscopy (TEM), X-ray diffraction (XRD), and electron backscattered diffraction (EBSD) were used to study the characteristics of the multiphase microstructure. The strengthening model of medium carbon multiphase steel was established on the relationship between phase fraction, phase constituents, and yield strength.

The influencing factors on mechanical properties of medium carbon multiphase steel are also revealed.

Experimental procedures

The chemical composition of the tested steel was 0.47C-0.32Mn-1.34Si-3.17Cr-1.27Mo-0.92 V-1.03Ni (wt.%). The test steel was prepared after vacuum smelting and electroslag remelting. The plate with thickness of 25 mm was obtained after hot rolling. Subsequently, the plate was subjected to spheroidizing annealing process, which was as follows: the plate was kept at 840 °C for 0.5 h, then after was held cooling for 15 min to 760 °C in furnace and then was kept for 1 h, and finally cooled to room temperature in furnace. The purpose of spheroidizing process is to obtain dispersed spherical undissolved carbides, and to reduce hardness, which is beneficial for cutting. Dilatometric measurements were carried out using a DIL805 dilatometer to examine the martensitic transformation temperature (M_S) and the kinetics of bainitic formation. When the sample was subjected to austenitizing at 1000 °C for 20 min, the M_S temperature was 295 °C. After the austenitizing process, two types of heat treatments were designed based on dilatometry test results. One is the bainitic austempering processes (BA): Directly cooled at M_S-40 °C (255 °C, BA-255), M_S-20 °C (275 °C, BA-275), $M_S + 20$ °C (315 °C, BA-315), and $M_S + 40$ °C (335 °C, BA-335) for 3.5 h, 2.9 h, 1.8 h, and 1.3 h, respectively. Then, samples were cooled to room temperature. The second was the martensitic quenching process: Directly quenched to room temperature by oil.

The microstructures of the samples were characterized by scanning electron microscopy (SEM, Hitachi SU-5000) and transmission electron microscopy (TEM, Talos F200x). SEM samples after mechanical polishing were etched with 4% nitric acid alcohol solution. The crystallographic orientations of the samples were determined by electron back-scattered diffraction (EBSD, OIM Collection 7.3 software). For EBSD analysis, the working voltage was 30 kV and the scanning step was 45 nm. TEM samples were ground mechanically down to 30 μm in thickness and then thinned by a TenuPol-5 dual-jet at 30 V in 7% perchlorate ethanol solution.

An X-ray diffractometer (XRD, Rigaku D/max-2500/PC) with unfiltered Cu $K\alpha$ radiation was used to measure the constituting phases. The samples were

step scanned with a scan rate of 2°/min ranging from 40° to 105°. The volume fraction of retained austenite (V_γ , %) [27] and the dislocation density of ferrite and retained austenite. (ρ , m^{-2}) [28] were determined using Eq. (1) and Eq. (2) with the integrated intensities of the (111) γ , (200) γ , (220) γ , and (311) γ peaks of austenite and the (110) α , (200) α , (211) α , and (220) α peaks of ferrite.

$$V_\gamma = \frac{1}{n} \sum_{j=1}^n \frac{I_\gamma^j}{R_\gamma^j} / \left(\frac{1}{n} \sum_{j=1}^n \frac{I_\gamma^j}{R_\gamma^j} + \frac{1}{n} \sum_{j=1}^n \frac{I_\alpha^j}{R_\alpha^j} \right) \quad (1)$$

where n is the number of peaks examined, and I is the integrated intensity of the diffraction peak. R is a material scattering factor, which can be expressed as: $R = \frac{1}{\sqrt{2}} F^2 P \frac{1+\cos^2 2\theta}{\sin\theta \sin 2\theta} e^{-2M}$. F is the structure factor, P is the multiplicity factor, e^{-2M} is the temperature factor.

$$\rho = \frac{k}{F} \cdot \frac{\varepsilon^2}{b^2} \quad (2)$$

where for body-centered cubic (bcc) phase, k equals to 14.4, $b = (\sqrt{3}/2)a$. For face-centered cubic (fcc) phase, k equals to 16.1, $b = (\sqrt{2}/2)a$. b is the dislocation Burgers vector, a is the lattice constant of bcc or fcc phase. The value of F is assumed to be 1. ε is microscopic strain, which was calculated using the Williamson–Hall equation, $\varepsilon = \frac{\delta}{4 \tan \theta} - \frac{K\lambda}{D \cos \theta}$, δ is the broadening of the peaks, K equals to 0.9, D is the crystallites size.

The tensile properties were measured by MTS test machine at a strain rate of 0.002 /s in accordance with a standard GB/T 228–2002. Plate samples, with a total length of 100 mm, a gauge length of 25 mm, and cross section of 10 \times 2 mm^2 , were used for tensile tests. The yield strength was determined by the 0.2% offset method. Impact properties were evaluated by U-notched Charpy impact samples with dimensions of 10 \times 10 \times 55 mm^3 . Three samples were tested under each condition. HR-150A Rockwell hardness tester was used to measure the hardness of the samples, and the average value was taken after ten times.

Results

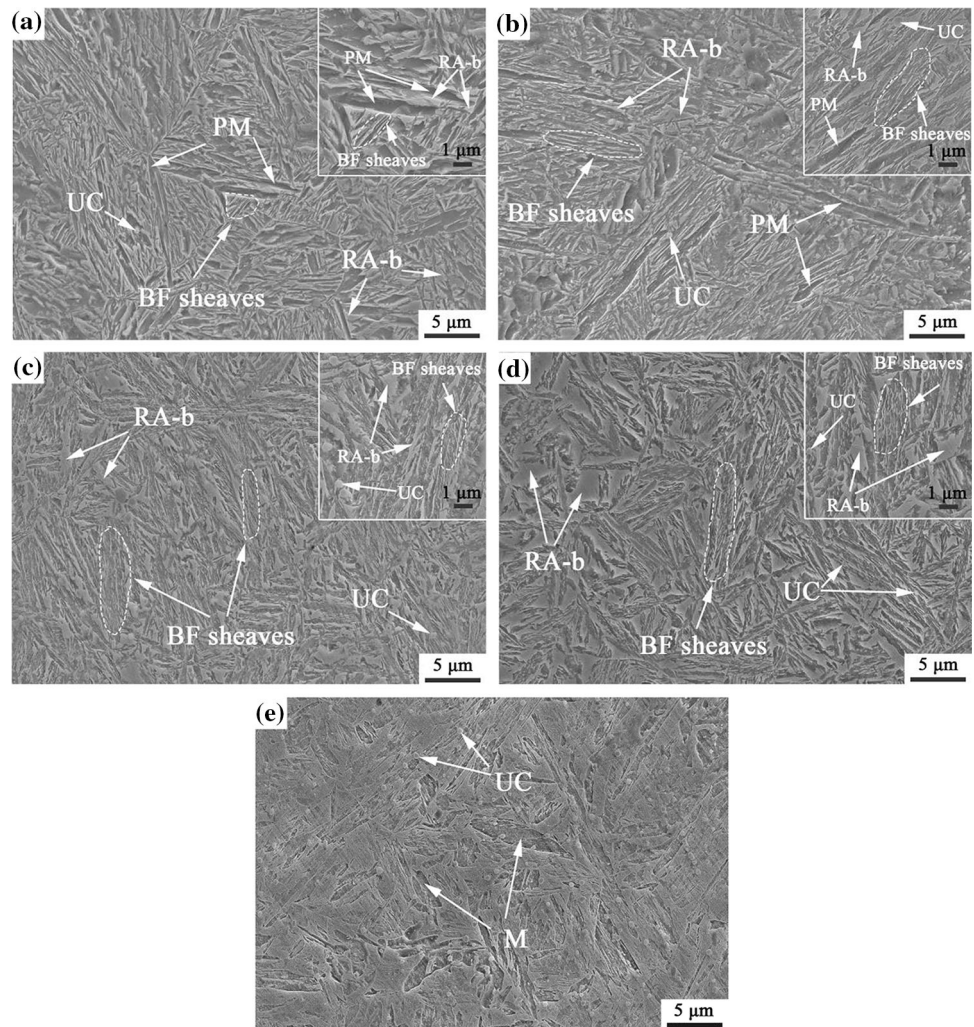
Microstructure

Figure 1 shows the SEM images of samples that were subjected to different heat treatment processes. The

microstructure of the above- M_S austempered samples consist of bainitic ferrite (BF) sheaves, blocky retained austenite (RA-b), and spherical undissolved carbides (UC). In contrast, in below- M_S austempered samples, the bainitic ferrite laths are distributed in different directions, and there is a certain amount of band-like pre-formed martensite (PM) (Figs. 1a,b). The direct-quenched sample consists of quenched martensite and spherical undissolved carbide (Fig. 1e). According to the microstructural difference, the microstructures the below- M_S (BA-255, BA-275) and above- M_S (BA-315, BA-335) austempered samples and direct-quenched sample are defined as PM-BF-RA (pre-formed martensite-bainitic ferrite-retained austenite), BF-RA (bainitic ferrite-retained austenite), and QM (quenched martensite), respectively. Since the volume fraction of UC in all samples was very small and the same, UC was not included in the naming.

According to statistics that were calculated using Image-Pro Plus software (IPP), the sizes of PM in the BA-255 and BA-275 samples were $0.75 \pm 0.14 \mu\text{m}$ and $0.78 \pm 0.12 \mu\text{m}$, respectively. Because the samples were treated with the same heat treatment process before the austempering process, all of the samples contain the same volume fraction of carbides. Specifically, the volume fraction of undissolved carbides is 1.2% according to the statistics. The size distribution of blocky retained austenite in austempered samples (Fig. 4a) can be obtained, and the average size can be calculated, the results are shown in Fig. 4d. With an increase in the austempering temperature, the size of blocky retained austenite increases; moreover, there is obviously larger blocky retained austenite in the BA-335 sample. However, there was no obvious blocky retained austenite in the QM sample.

Figure 1 SEM micrographs of samples subjected to different heat treatments: **a** BA-255 sample, **b** BA-275 sample, **c** BA-315 sample, **d** BA-335 sample, and **e** QM sample.



EBSD was used to characterize the microstructure of the austempered and direct-quenched samples. Figure 2 shows the inverse pole figure (IPF) of the samples. Crystallographic theory is used to reconstruct the hierarchical structure of block and packet of bainite or martensite using the MTEX toolbox in MATLAB [29]. The Kurdjumov–Sachs (K-S) orientation relationship is used here. Black and white lines represent the boundaries of blocks and packets, respectively. A packet contains 6 ~ 15 blocks in the PM-BF-RA samples, 5 ~ 10 blocks in the BF-RA samples, and 4 ~ 8 blocks in the QM sample. The distribution of block sizes was measured according to the reconstructed hierarchical structure (Fig. 4b), the average size was calculated, and the results are shown in Fig. 4d. Compared with the QM sample, the average sizes of blocks in the austempered samples were smaller. Moreover, the sizes of blocks in the PM-BF-RA samples were smaller than those in the BF-RA samples, and this indicates that PM significantly refines the bainitic microstructure.

Figure 3 shows TEM microstructure of samples that were subjected to different heat treatment processes. The bainitic ferrite sheaves of austempered samples are all composed of bainitic ferrite laths and thin film retained austenite (RA-f), and bainitic ferrite

laths have a K-S relationship with the retained austenite. Moreover, it is observed that band-like PM is present in the PM-BF-RA samples. The QM sample consists of lath-shaped quenched martensite. IPP software was used to measure the mean linear intercept in a direction normal to the length of lath of bainitic ferrite, thin film retained austenite, and quenched martensite. According to Eq. (3), the stereological correction of lath of bainitic ferrite, thin film retained austenite, and quenched martensite was carried out [30]. Also, the distribution of the lath thickness for bainitic ferrite in the austempered sample was obtained by statistics (Fig. 4c), and the average thickness of the laths for all the samples was finally obtained, as shown in Fig. 4d.

$$t_i = 2L_i/\pi \quad (3)$$

where i represents the phases (bainitic ferrite, thin film retained austenite, and quenched martensite), L_i is the mean linear intercept of phases and t_i is the thickness of lath of phases.

With an increase in austempering temperature, the thickness of bainitic ferrite lath and thin film retained austenite increases, which is consistent with the results in the literature [7, 8]. Compared with the thickness of bainitic ferrite lath in the austempered

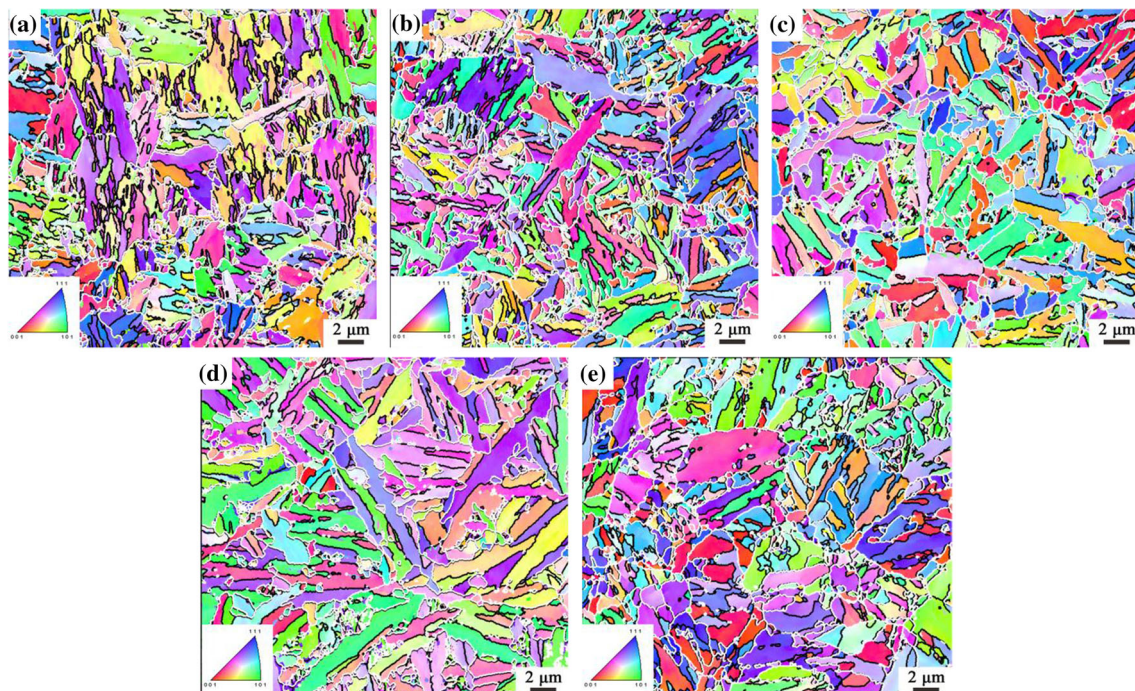


Figure 2 IPF micrographs of samples subjected to different heat treatments: **a** BA-255 sample, **b** BA-275 sample, **c** BA-315 sample, **d** BA-335 sample, and **e** QM sample. Note: Black lines: boundaries of blocks; white lines: boundaries of packets.

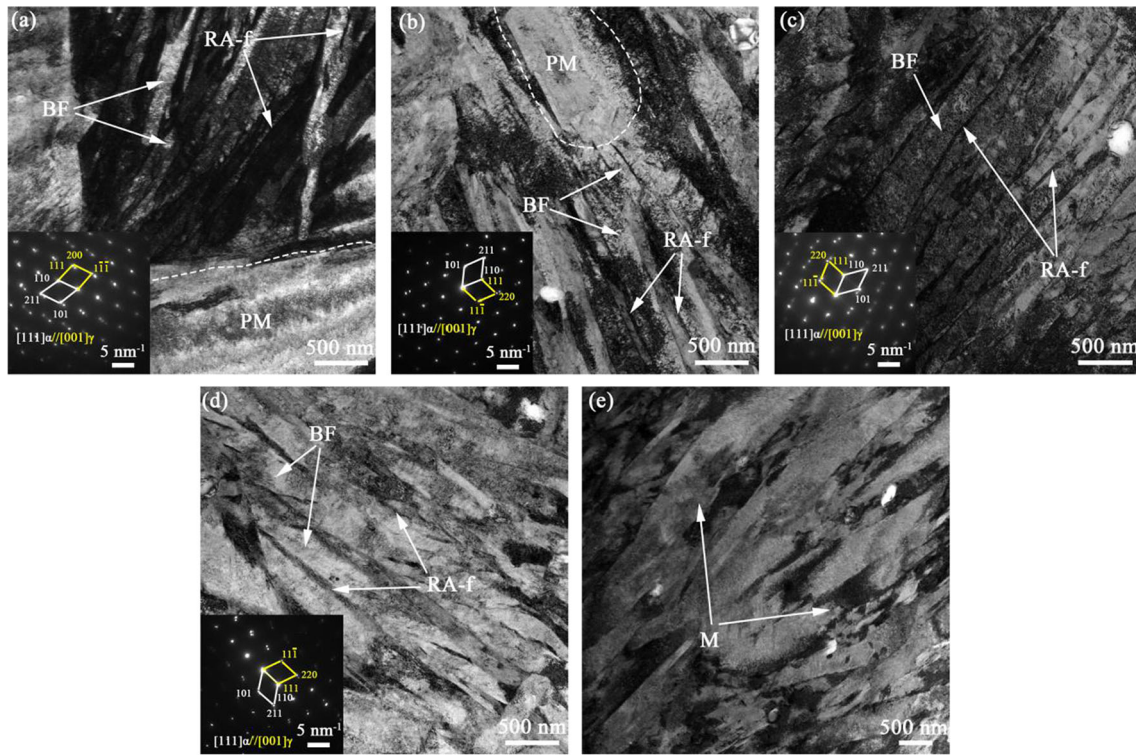


Figure 3 TEM micrographs of samples subjected to different heat treatments: **a** BA-255 sample, **b** BA-275 sample, **c** BA-315 sample, **d** BA-335 sample, and **e** QM sample.

sample, the thickness of quenched martensitic lath is obviously coarser (Fig. 3g). In addition, the thickness of the bainitic ferrite lath in PM-BF-RA samples is thinner than that in BF-RA samples, which demonstrates that PM significantly refines bainitic ferrite lath. Moreover, the refinement rule of bainitic ferrite lath is same as that of the blocks' size shown in Fig. 4d.

Phase analysis

The expansion strain–temperature curves of PM-BF-RA and BF-RA samples during the final cooling after austempering were measured using dilatometer (Fig. 5). For PM-BF-RA samples, a deviation from linearity occurs during cooling from M_s to the austempering temperature. This deviation indicates the formation of PM. Once the austempering temperature is reached, the vertical increase of strain takes place in the PM-BF-RA and BF-RA samples, which is related to the formation of bainitic ferrite (BF). Furthermore, the slope of the line does not change during the final cooling after austempering, which indicates that no fresh martensite (FM) forms

during final cooling in all samples. Moreover, similar results have been reported in other studies [11, 17].

Figure 6a shows XRD patterns of the samples that were subjected to different heat treatment processes. The austempered and quenched samples are mainly composed of the ferrite phase and austenite phase. The integrated area of the austenite peak in the austempered sample is much larger than that in the quenched sample, which illustrates that there is more retained austenite in the austempered sample. According to Eq. (1) and (4), the volume fraction of retained austenite (V_γ) and PM (V_{PM}) were calculated, respectively, and the volume fraction of bainitic ferrite (V_B) can be obtained. The volume fraction of each phase in samples with different heat treatment processes is shown in Fig. 6b. With an increase in the austempering temperature, the volume fraction of retained austenite in the austempered samples increases. Moreover, PM-BF-RA samples contain less bainitic ferrite and retained austenite than BF-RA samples.

$$V_{PM} = 1 - \exp^{-1.1 \times 10^{-2}(M_s - AT)} \quad (4)$$

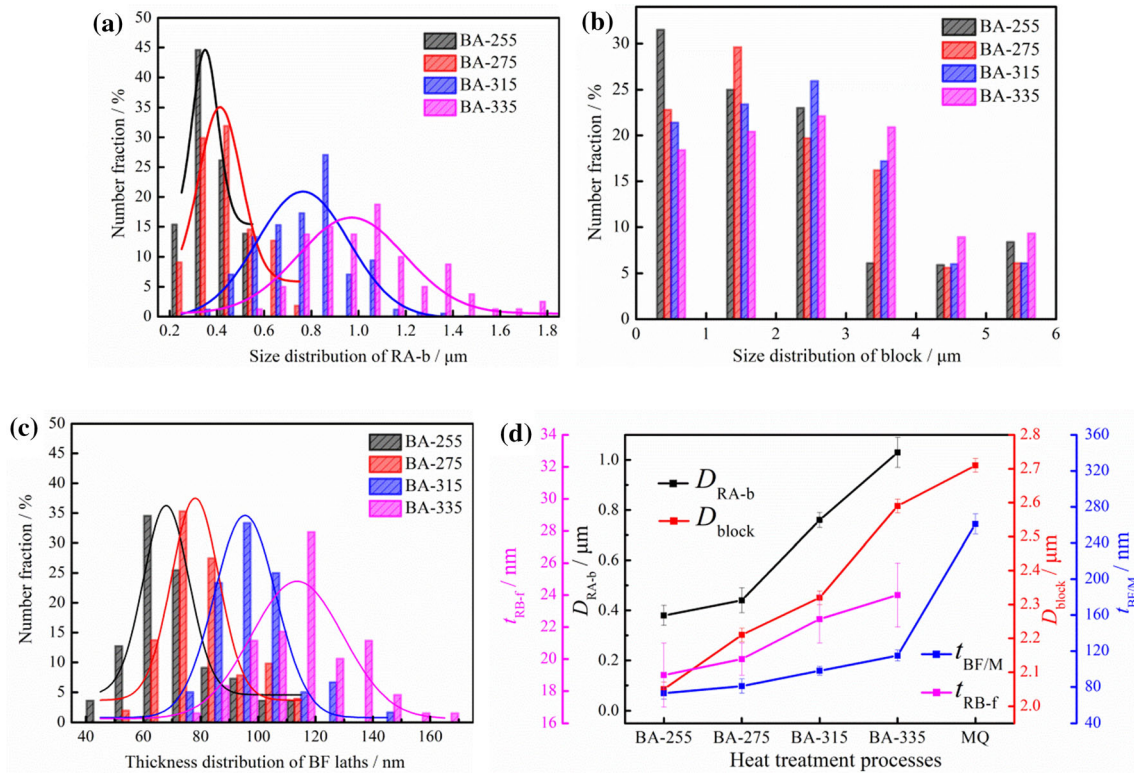


Figure 4 Size distribution of **a** blocky retained austenite, **b** a block of bainite, and **c** bainitic ferrite in the austempered samples, and **d** Average size of blocky retained austenite (D_{RA-b}), a block of

bainite (D_{block}), bainitic ferrite (t_{BF}), martensite (t_M), and film retained austenite (t_{RA-f}).

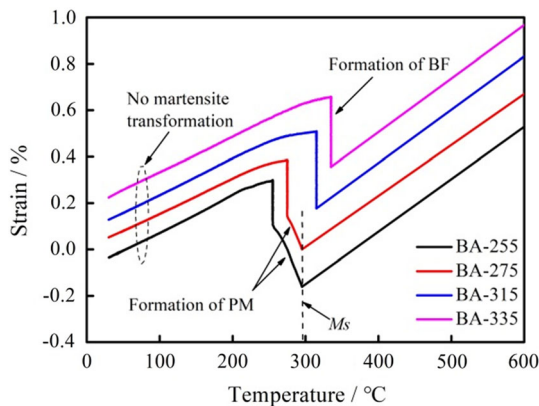


Figure 5 The expansion strain–temperature curves of samples subjected to different heat treatments.

where AT is the austempering temperature, which is lower than M_s [31].

The dislocation density of bainitic ferrite, retained austenite, and martensite was calculated according to Eq. (2). The dislocation density of the QM sample was significantly higher than that of the austempered sample. Moreover, with an increase in the austempering temperature, the dislocation density of bainitic

ferrite and retained austenite gradually decreased. The carbon content of the retained austenite was calculated according to Eq. (5) [32], and the data are shown in Table 1.

$$C_\gamma = (a_\gamma - 3.578)/0.033 \tag{5}$$

where C_γ is the carbon content of retained austenite, a_γ is the lattice constant of retained austenite.

To visually compare the changes of retained austenite in PM-BF-RA and BF-RA samples, Fig. 7a shows the $(200)_\gamma$ diffraction peak of retained austenite in austempered samples. Compared with BF-RA samples, the integrated area of $(200)_\gamma$ diffraction peak of retained austenite in PM-BF-RA samples is smaller, and the 2θ angle of $(200)_\gamma$ is shifted to the left. This indicates that the volume fraction of the retained austenite is smaller but its carbon content is higher in PM-BF-RA samples, which corresponds to the volume fraction of retained austenite and its carbon content calculated in Table 1.

Two types of retained austenite with different carbon content can be obtained during the austempering process [1, 7]. The different carbon content in

Figure 6 **a** XRD patterns and **b** volume fractions of phases in samples subjected to different heat treatment processes.

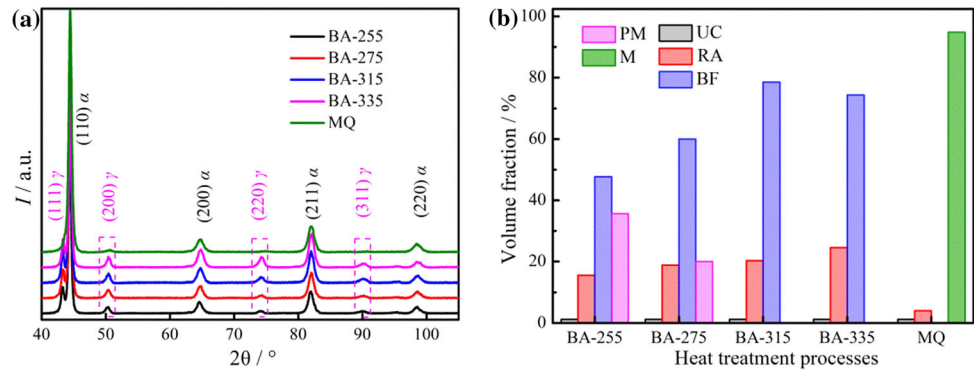


Table 1 Results of XRD analysis

Heat treatment process	RA _i	2θ-RA _i /°	C _{RAi} /wt.%	V _{RAi} /V _{RA}	ρ _α /10 ¹⁵ m ⁻²	ρ _γ /10 ¹⁵ m ⁻²	V _{RA} /%	2θ-RA/°	C _{RA} /wt.%
BA-255	RA ₁	50.09	1.88	0.37	6.17	10.40	15.5	50.29	1.45
	RA ₂	50.33	1.41	0.63					
BA-275	RA ₁	50.26	1.51	0.46	6.13	9.16	18.9	50.38	1.26
	RA ₂	50.40	1.21	0.54					
BA-315	RA ₁	50.28	1.48	0.58	6.01	7.70	20.3	50.44	1.08
	RA ₂	50.48	1.08	0.42					
BA-335	RA ₁	50.41	1.22	0.57	5.70	6.67	24.6	50.52	0.98
	RA ₂	50.54	0.94	0.43					

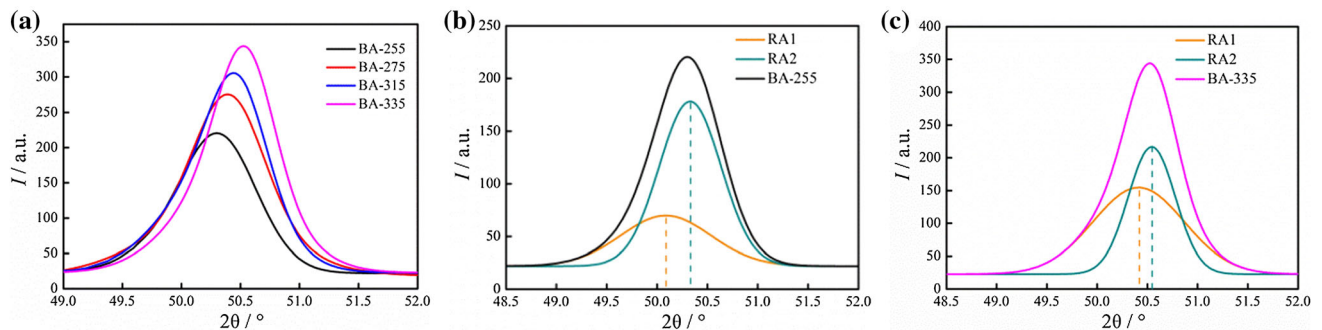


Figure 7 **a** (200)γ peaks of the austempered samples, **b, c** Gaussian fitting of (200)γ peaks in BA-255 sample and BA-335 sample.

the two types of retained austenite leads to the asymmetry of austenite diffraction peaks [33]. The Gaussian multi-peaks fitting method can be used to divide the retained austenite into a high-carbon austenite region (RA1) and a low-carbon austenite region (RA2) [34, 35]. Figure 7b,c shows the curves of (200)γ Gaussian fitting peaks of PM-BF-RA sample (BA-255 sample) and BF-RA sample (BA-335 sample). The carbon contents of the high-carbon region (C_{RA1}), low-carbon region (C_{RA2}), and overall retained austenite (C_{RA}) of the austempered sample were calculated according to Eq. (5), and the results are

shown in Table 1. Compared with BF-RA samples, PM-BF-RA samples have a high-carbon austenite region that is smaller than the low-carbon austenite region. It is worth noting that the retained austenite contains high-carbon content in PM-BF-RA samples, even in the low-carbon austenite region, the carbon content is higher than 1.2 wt.% (Table 1), which is higher than the high-carbon retained austenite region of BF-RA samples.

Mechanical properties

Figure 8 shows the engineering stress–strain curves of samples with different heat treatment processes (Fig. 8a), the amplified view of the engineering stress–strain curves (Fig. 8b), and the statistics diagram of hardness and impact energy (Fig. 8c). Compared with QM sample, the austempered samples have lower strength and hardness, but its plasticity and toughness are obviously higher. For the austempered sample, the hardness, yield strength, and impact energy of the austempered samples gradually decreased with an increase in the austempering temperature; however, the tensile strength did not change significantly.

Compared with BF-RA samples, PM-BF-RA samples exhibit higher yield strength, hardness, and plasticity. It is worth noting that the BA-275 sample has optimal comprehensive mechanical properties. Compared with the BA-335 sample, the hardness, the impact energy, and the product of strength and elongation increase by 4.5%, 26.7%, 20.8% in the BA-

275 sample, respectively. The effect that multiphase microstructure has on mechanical properties will be discussed in the following section.

Discussion

Different phases (PM, M, BF, and RA) and the microconstituents in each phase (e.g., the dislocation density or the size) can affect the mechanical properties of bainitic multiphase steel. The following sections will discuss the microstructural characteristics of different multiphase structures and a quantitative evaluation of the mechanical properties by phase fraction and microconstituents of phases.

Microstructural features

As mentioned above, compared with the BF-RA samples, the size of bainitic block in the same packet is smaller and there are more bainitic blocks in the PM-BF-RA samples. Moreover, the block contains

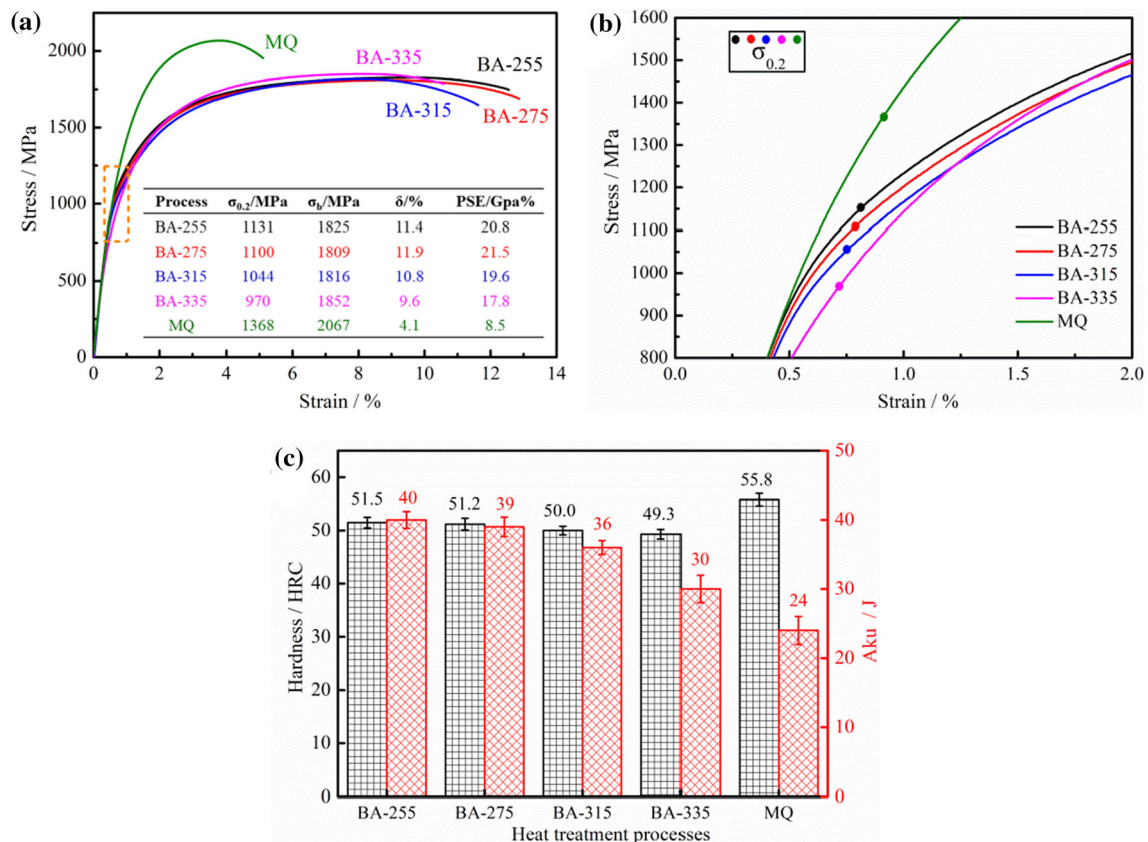


Figure 8 a Engineering strain–stress curve, b Amplified view of the engineering stress–strain curves (marked Orange dashed rectangle in a), c Hardness and impact energy. Note $\sigma_{0.2}$: yield strength, σ_b : tensile strength, δ : elongation, PSE: product of strength and elongation.

subunits, such as bainitic ferrite laths, and the refinement of the block is accompanied by the refinement of bainitic ferrite laths (Fig. 4d). The reasons for this result are as follows: These results are mainly related to the nucleation and growth of bainitic ferrite and to the strength of undercooled austenite. The nucleation driving force curve for this tested steel was calculated using Mucg83 software [36], and the results (red line) are shown in Fig. 9. The below- M_s austempering temperature results in large undercooling, which causes a large driving force of the bainite transformation and to more bainite nucleation sites [7, 13]. When the austempering temperature is lower, the strength of supercooled austenite is greater, which leads to refinement of bainitic ferrite lath [37]. The refinement of bainitic ferrite lath is also related to the introduction of PM in the multiphase structure. PM tends to divide the grain of the original austenite. This increases the nucleation sites and promotes nonuniform nucleation of bainitic ferrite, which can refine the bainitic ferrite lath [38, 39]. Moreover, plastic and elastic strains are introduced into the surrounding undercooled austenite after PM forms, this increases the strength of the undercooled austenite, which increases the shear effect resistance of bainite transformation and reduces the critical nucleation size of bainitic ferrite [18, 39]. In summary, the size of the bainitic block and the thickness of bainitic ferrite lath are significantly refined in PM-BF-RA samples.

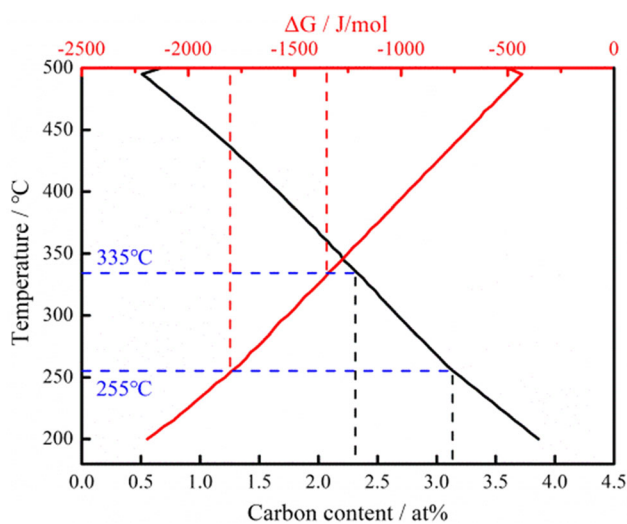


Figure 9 T_0' curves (Black line) and the relationship between the free energy and temperature (Red line), calculated by Mucg83 software.

With an increase in the austempering temperature, the volume fraction of the retained austenite gradually increases (Table 1), and the influencing factors are as follows. According to T_0' theory, when the carbon content in untransformed austenite reaches the carbon content defined by the T_0' curve, the free energy change between bainitic ferrite and austenite is no longer greater than the elastic energy barrier; thus, the bainite transformation cannot occur [23, 37]. The T_0' curve of this tested steel was calculated using Mucg83 software, and the result (black line) is shown in Fig. 9. As seen, the carbon content defined by the T_0' curve gradually decreases with an increase in the austempering temperature. In general, the diffusion rate of carbon atoms is relatively high at a higher austempering temperature, and carbon tends to diffuse from bainitic ferrite to surrounding austenite. Thus, the carbon content in austenite more easily reaches the defined value that corresponds to the austempering temperature in the T_0' curve. Therefore, the volume fraction of retained austenite in the sample that had a higher austempering temperature is higher at the end of the transformation. In other words, PM-BF-RA samples contain less retained austenite than BF-RA samples.

As for the size of blocky retained austenite in the microstructures, the size of undercooled austenite can be reduced due to the introduction of PM in PM-BF-RA samples, and finally, small-sized blocky austenite can be obtained [13, 17]. Moreover, there are many nucleation sites in the PM-BF-RA samples during bainite transformation. Also, bainitic ferrite laths grow in different directions, and this further divides the untransformed austenite into smaller sizes. Therefore, as mentioned in Sect. 3.1, the size of blocky retained austenite is smaller in PM-BF-RA samples than in BF-RA samples. In addition, the carbon content of retained austenite in PM-BF-RA samples is higher than that in BF-RA samples. In the austempering process, the carbon atoms in PM can be discharged into the dislocation position or the surrounding retained austenite, so that retained austenite with high stability can be obtained [40]. Moreover, it is well known that carbon can be discharged into the surrounding untransformed austenite after bainitic ferrite laths form in different directions, which results in blocky retained austenite between bainitic ferrite laths in different directions more easily enriching carbon [7]. In addition, when the distance between the interface of PM or bainitic ferrite and the

center of blocky austenite is shorter, the carbon atoms diffuse more easily to the center of blocky retained austenite. Therefore, blocky austenite with a smaller equivalent size in PM-BF-RA samples can easily achieve carbon enrichment and a uniform distribution.

Strengthening mechanism of multiphase microstructure

There are significant differences between the mechanical properties of PM-BF-RA and BF-RA samples (Fig. 8), and this can be explained by considering the contributions that the different strengthening mechanisms have on yield strength. According to the volume fraction of the phase and the difference of microconstituents of each phase, a model based on the studies was established [19–22]. This model was used to estimate the yield strength of steels according to the volume fraction of multiphase and the microconstituents of phases. The calculation formula of the yield strength of the three-phase mixed microstructure is defined as Eq. (6):

$$\sigma_{0.2}^{\text{calculate}} = \sum f_i \times \sigma_i \quad (6)$$

where $\sigma_{0.2}^{\text{calculate}}$ represents the calculated yield strength of the sample, f_i represents the volume fraction of each phase, σ_i is the calculated yield strength of the unit volume fraction phase, and i represents the phase (bainitic ferrite, retained austenite, and PM). In addition, it has been shown in literature that only carbides with small size (less than 100 nm) can produce effective precipitation strengthening [41]. In this paper, the average size of UC is 328 ± 16 nm; thus, precipitation strengthening contribution was assumed as zero.

Considering the interaction between the microconstituents of a single phase, (i.e., the entanglement of dislocations, the strengthening of solute particles and the effect of grain size), the linear superposition of multiple strengthening modes of a single phase in the literature is not applicable here [9]. Therefore, a combination of linear superposition and a root mean square model can be used to calculate the strength contributions by considering the overlap effect of each strengthen contributors, the yield strength of three phases mentioned above (PM, BF, RA) is calculated by Eq. (7) [42]:

$$\sigma_i = \left((\sigma_0 + \sigma_g^i + \sigma_s^i)^2 + (\sigma_d^i)^2 \right)^{1/2} \quad (7)$$

where σ_0 is the friction stress of pure iron single crystal, about 53.9 MPa [43]. σ_g^i , σ_s^i and σ_d^i are the contributions of solid solution strengthening, grain boundary strengthening, and dislocation strengthening of each phase, respectively. In addition, the yield strength is calculated according to parameters of each phase's microconstituents in PM-BF-RA and BF-RA samples.

Strength of bainitic ferrite

Solid solution strengthening Solid solution strengthening is determined by the percentage of alloying elements that are dissolved into the matrix. The following empirical equation (Eq. (8)) is used to calculate the contribution of solid solution strengthening [44]:

$$\sigma_s^{BF} = 1722.5 \times w_C^{1/2} + 32w_{Mn} + 84w_{Si} + 3w_V + 11w_{Mo} - 30w_{Cr} \quad (8)$$

where σ_s^{BF} is the contribution of solute elements in bainitic ferrite to solid solution strengthening. The alloying elements (Mn, Si, V, Mo, Cr) were selected, wt.%. The literature shows that carbon content in bainitic ferrite is only 0.03 wt.%, slightly higher than the equilibrium state [7]. The contribution of solid solution strengthening of bainitic ferrite in PM-BF-RA and BF-RA samples was 397 MPa (Fig. 10a).

Grain boundary strengthening The strengthening unit of nanobainite microstructure is bainitic ferrite lath, and so the thickness of bainitic ferrite is selected for the calculations. Because the thickness is less than 200 nm, the grain refinement strengthening can be estimated using Langford type [45].

$$\sigma_g^{BF} = k_1 \times (2t)^{-1} \quad (9)$$

where k_1 is a constant, 115 MPa· μm , t is the thickness of bainitic ferrite, μm . From calculations, it is determined that the contribution that bainitic ferrite makes to grain boundary strengthening gradually decreases with an increase in the austempering temperature. Moreover, the grain boundary strengthening contribution of bainitic ferrite in PM-BF-RA samples is

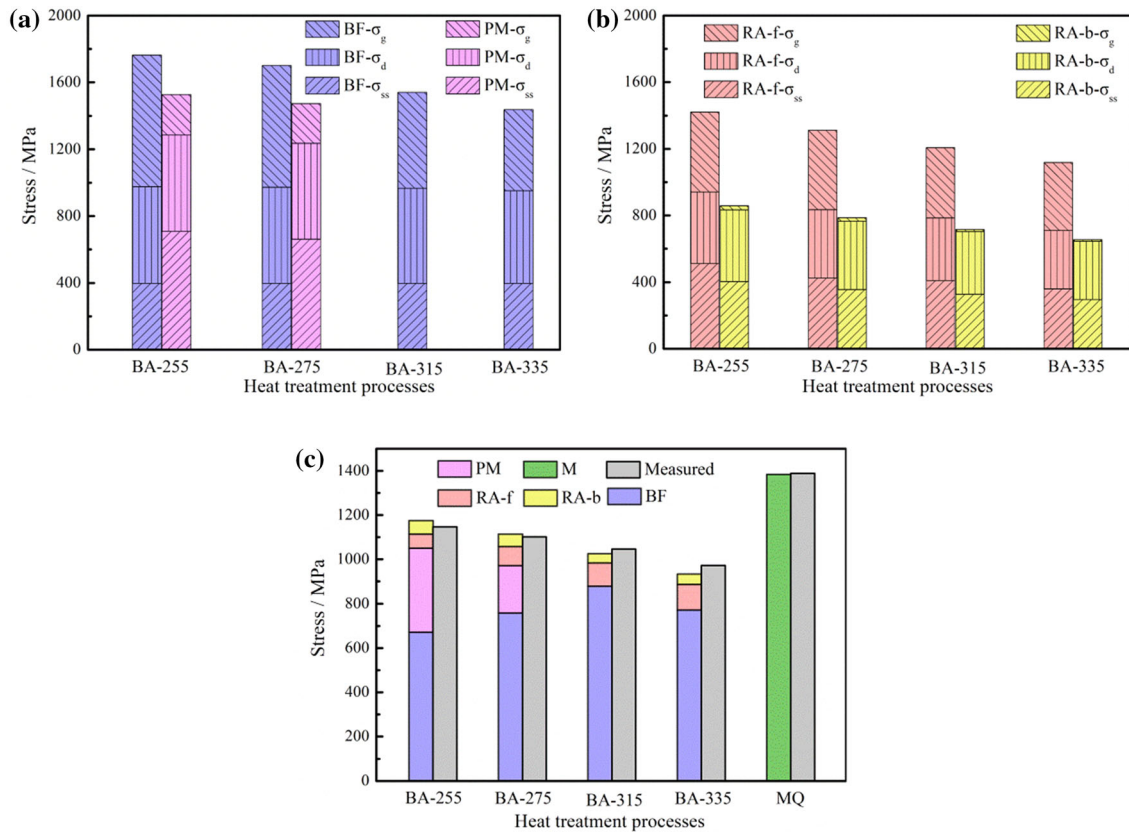


Figure 10 **a** Strengthening mechanism of unit volume bainitic ferrite and PM, **b** strengthening mechanism of unit volume film and blocky retained austenite, and **c** comparison of the sum of contributions of different phases to yield strength with

significantly higher than that in BF-RA samples (Fig. 10a).

Dislocation strengthening According to the dislocation density in bainitic ferrite (Table 1), the contribution that dislocation makes to yield strength can be estimated using the Williamson–Hall method [20]:

$$\sigma_d^{BF} = C \times \sqrt{\rho} \tag{10}$$

where C is 7.34×10^{-6} MPa/m, ρ is dislocation density, $/m^{-2}$. The calculation shows that the dislocation strengthening contribution of bainitic ferrite in PM-BF-RA samples is slightly higher than that in BF-RA samples (Fig. 10a).

For bainitic ferrite phase, grain boundary strengthening and dislocation strengthening are the dominant strengthening mechanisms (Fig. 10a). Because of the thinner thickness of bainitic ferrite lath and the greater dislocation density in PM-BF-RA samples, the corresponding grain boundary

experimental strength. Note σ_{ss} , σ_g and σ_d are the contributions of solid solution strengthening, grain boundary strengthening, and dislocation strengthening of each phase, respectively.

strengthening and dislocation strengthening make great contributions.

Strength of pre-formed and quenched martensite

PM and quenched martensite were obtained after different heat treatment processes. There are different microconstituents in two types of martensite. In order to compare of the strengthening contribution of PM and quenched martensite, the microconstituents parameters in two types of martensite were calculated here.

Solid solution strengthening The solution strengthening of PM and quenched martensite was calculated using Eq. (11) [46]. The carbon content in tempered martensite that subjected to the same temperature–time condition as the below- M_s austempering process will be considered as the carbon content of PM in the below- M_s austempered samples [19]. Thus, the

carbon content of tempered martensite formed in tempering treatments at temperatures of 255 °C and 275 °C (below M_s) can be considered as the carbon content of PM in BA-255 and BA-275 samples, respectively.

$$\sigma_s^{M/PM} = 1171.3 \times w_C^{1/3} + 32w_{Mn} + 84w_{Si} + 3w_V + 11w_{Mo} - 30w_{Cr} \quad (11)$$

where the concentration of carbon, manganese, silicon, vanadium, molybdenum, chromium in martensite phase is in wt. %.

The carbon content in quenched martensite or PM is calculated using Eq. (12) with the lattice constant of its body-centered cubic structure [47].

$$C^{M/PM} = s \times (a^{M/PM} - a^\alpha) \quad (12)$$

where $C^{M/PM}$ is the carbon content of quenched martensite or PM, s is a constant, the value is 31 wt. %/Å, $a^{M/PM}$ is the lattice parameter of the quenched martensite or PM, and a^α is the lattice parameter of containing no carbon in the BCC phase, with a value of 2.866 Å. The carbon content of quenched martensite was calculated to be 0.32 wt. %. The carbon content of PM in BA-255 and BA-275 samples was calculated to be 0.14 wt.% and 0.11 wt.%, respectively. The calculated results show that the contributions of solid solution strengthening of PM in BA-255 and BA-275 samples are 707 MPa and 660 MPa, respectively. The contribution of solution strengthening of quenched martensite in QM samples is 900 MPa (Fig. 10a).

Grain boundary strengthening The sizes of quenched martensite and PM are both more than 200 nm, and the grain strengthening can be estimated using the Hall–Petch equation, which is applicable for sub-micron grains [48].

$$\sigma_g^{M/PM} = k_2 \times d^{-1/2} \quad (13)$$

where k_2 is a constant, 0.21 MPa·m^{1/2}, d is the average grain size, μm. The values of the grain boundary strengthening contribution of PM in the BA-255 and BA-275 samples are 243 and 239 MPa, respectively. The grain boundary strengthening contribution of quenched martensite in the QM sample is 411 MPa (Fig. 10a).

Dislocation strengthening Although the morphologies of martensite and bainite are different, the

structures are both body-centered cubic. Thus, the dislocation strengthening formula that is used to calculate the yield strength of quenched martensite and PM can be the same as that for calculating the yield strength of bainitic ferrite, namely Eq. (10). The values of the dislocation strengthening contribution of PM in the BA-255 and BA-275 samples are 578 MPa and 575 MPa, respectively. The dislocation strengthening contribution of quenched martensite in the QM sample is 637 MPa (Fig. 10a). Compared with the bainitic ferrite phase, the main strengthening mechanisms of the martensite phase (PM and quenched martensite) are solution strengthening. However, because of the large thickness of the lath, the contribution of grain boundary strengthening is relatively small. The carbon content of PM in PM-BF-RA samples is relatively lower than those in quenched martensite, and this results in lower contributions from the solid solution strengthening.

Strength of retained austenite

Two kinds of retained austenite are present in PM-BF-RA and BF-RA samples: one is thin film retained austenite with high-carbon content (RA-f), and the other is blocky retained austenite with low-carbon content (RA-b). Moreover, the size of thin film retained austenite is smaller than the blocky retained austenite [1, 7, 10]. The microconstituent parameters (e.g., the size and carbon content) of the two kinds of retained austenite are different. Hence, the yield strength of the two kinds of retained austenite must be calculated separately. In addition, because both retained austenite samples are in a face-centered cubic phase, the same formulas can be used to calculate the yield strength of the two kinds of retained austenite. The volume content of retained austenite in the QM sample is less than 4%, the influence that it has on mechanical properties can be ignored, and thus, the contribution of retained austenite to yield strength is not calculated.

Solid solution strengthening The yield strength of retained austenite can be estimated according to Eq. (14) [37]:

$$\begin{aligned} \sigma_s^{RA-f/b} = & 15.4 \times (1 - 0.26 \times 10^{-2}T_r + 0.47 \times 10^{-5}T_r^2 \\ & - 0.326 \times 10^{-8}T_r^3) \times (4.4 + 23w_c + 1.3w_{Si} \\ & + 0.24w_{Cr} + 0.94w_{Mo}) \end{aligned} \tag{14}$$

where the concentration of carbon, manganese, silicon, vanadium, molybdenum, chromium in martensite phase is in wt.%, $T_r = T-25$, T is austempering temperature, °C. From calculations, it is determined that the solid solution strengthening contribution of retained austenite decreases with an increase in the austempering temperature. Moreover, the solid solution strengthening contribution of retained austenite in PM-BF-RA samples was significantly higher than that in BF-RA samples (Fig. 10b).

Grain boundary strengthening The grain boundary strengthening effect of retained austenite can be estimated using Eq. (15) [10].

$$\sigma_s^{RA-f/b} = \frac{\alpha M \mu b}{t_{RA-f/b}} \tag{15}$$

where α is a quantitative factor with a value of 0.23, M is Taylor factor with a value of 2.2, μ is shear modulus, 75 GPa, b is the dislocation Burgers vector with a value of 0.248 nm, $t_{RA-f/b}$ is the size of thin film or blocky retained austenite. The contribution of grain boundary strengthening of blocky retained austenite in PM-BF-RA samples was calculated and is found to be higher than that of BF-RA samples. The size of film austenite in PM-BF-RA and BF-RA samples is similar, and thus, the contribution of the grain boundary strengthening does not change significantly (Fig. 10b).

Dislocation strengthening To coordinate the phase transformation, a large number of dislocations exist in austenite. Therefore, dislocation strengthening should be considered [48].

$$\sigma_d^{RA-f/b} = \alpha \mu b \sqrt{\rho_{RA}} \tag{16}$$

where α , μ , b are the same as those in Eq. (15), and ρ_{RA} is the dislocation density of retained austenite. Here, it is assumed that blocky retained austenite and film retained austenite have the same the dislocation density in the same treatment process. From calculations, it is found that the contribution of dislocation strengthening of retained austenite gradually decreases with an increase in the austempering

temperature. Moreover, the dislocation strengthening contribution of retained austenite in PM-BF-RA samples is slightly higher than that in BF-RA samples (Fig. 10b).

In film retained austenite, solid solution strengthening and the grain boundary are the dominant strengthening mechanism, and in blocky retained austenite, solid solution strengthening is the dominant strengthening mechanism (Fig. 10b). The yield strength of retained austenite depends on its size and carbon content. The size and carbon content of thin film retained austenite are significantly higher than those of blocky retained austenite, which results in high contribution of solid solution strengthening and grain boundary strengthening. In addition, although the carbon content of retained austenite in PM-BF-RA samples is significantly higher than that in BF-RA samples, volume fraction of retained austenite in PM-BF-RA samples is smaller, leading to the contribution of its retained austenite to the strength is similar to that in BF-RA samples.

As seen in Fig. 10c, the difference between the calculated value of the yield strength and the actual value with different processes were used is 14 MPa ~ 37 MPa (1.3% ~ 3.8%). The strengthening model of multi-phases and multi-parameters is established in this paper, and it matches well with the actual yield strength. From a comprehensive comparison of the relationship between different phases in the microstructure and the contribution of yield strength, it can be concluded that bainitic ferrite is the dominant phase of yield strength in PM-BF-RA and BF-RA samples, and the contribution to the yield strength of bainitic ferrite in PM-BF-RA and BF-RA samples is 58–69% and 83–86%, respectively. The contribution to the yield strength of PM in PM-BF-RA samples is in the range of 19% ~ 32%. Moreover, the contribution that bainitic ferrite and pre-formed martensite make to yield strength is in the range of 88% ~ 90% in PM-BF-RA samples, this is higher than that of bainitic ferrite single phase in BF-RA samples.

Moreover, from comprehensive analysis, it is determined that the fine size and high dislocation density of bainitic ferrite and the high-carbon content of PM are important phase microconstituent parameters that lead to high yield strength of PM-BF-RA samples. The strengthening mechanism that corresponds to the above parameters dominates the yield strength. For BF-RA samples, the fine size of bainitic

ferrite is an important phase microconstituent parameter. In addition, the dominant phase of the yield strength in the QM sample is quenched martensite.

Work hardening behavior

The strain stage of the TRIP effect of retained austenite can be roughly observed in the work hardening rate curve. The work hardening rate curve of samples that were subjected to different processes is shown in Fig. 11. Compared with the austempered sample, the QM sample has higher work hardening rate when the strain is less than 0.021 (Fig. 11a, A1). However, when the strain is greater than 0.021, the work hardening rate of QM sample decreases rapidly (Fig. 11a), because the QM sample has a smaller amount of retained austenite, the TRIP effect cannot occur effectively. The work hardening rate curve of the austempered sample can be divided into three stages. In the first stage, the strain is less than 0.004 (Fig. 11b, A2). In this stage, the work hardening rate of PM-BF-RA samples is higher than that of BF-RA samples. This process is related to the density and uniform distribution of dislocations and to the inelastic behavior of dislocation segment bending [49, 50]. As mentioned above, there are high-density dislocations in the PM in PM-BF-RA samples, and the dislocations are introduced into the nearby bainitic ferrite and retained austenite. Therefore, a large number of dislocations proliferate and become tangled under low strain in PM-BF-RA samples, resulting in higher initial work hardening rate. In the second stage, the strain is in the range of 0.004 ~ 0.0748. It is noteworthy that the work-hardening rate of the BA-335 sample is significantly higher than that of other samples when the strain is

0.0059 (Fig. 11b, A3). The blocky retained austenite in the BA-335 sample has lower carbon content and larger size. Thus, it is easy to transform this blocky retained austenite into stress-induced martensite during further tensile deformation. Therefore, BF-RA samples had a high work hardening rate in the second stage. In the third stage, the strain is 0.0748 ~ 0.12. In this stage, the work hardening rate of PM-BF-RA samples is higher than that of BF-RA samples. The retained austenite that has high-carbon content and small size continuously produces the TRIP effect in the tensile process and delays the occurrence of necking, which is conducive to improving the material plasticity [7, 17, 23]. When the strain exceeds 0.0748 (Fig. 11c, A4), the stress-induced martensite produced by the TRIP effect in BF-RA samples accelerates the initiation and propagation of microcrack during the tensile process. This causes a loss of the protective effect on necking, and thus, the work hardening rate of the microstructure decreases rapidly. For PM-BF-RA samples, the blocky retained austenite with high-carbon content and small size exhibits high mechanical stability; this leads to a continuous TRIP effect with an increase in strain and results in a delay in necking and an increase in elongation.

It is reported in the literature that higher volume fraction of retained austenite is necessary for obtaining higher elongation [25, 26]. However, in this paper, although BF-RA samples contain higher volume fraction of retained austenite, its elongation is lower than that of PM-BF-RA samples. This demonstrates that the carbon content and size of retained austenite in bainitic steel that has a multiphase microstructure are more important than the volume fraction for improving the elongation. Also, the two phases (PM and bainitic ferrite) in PM-BF-RA

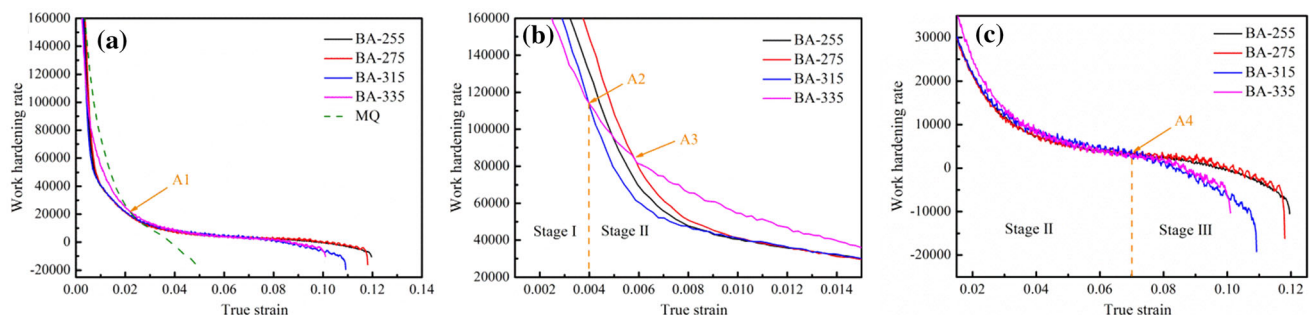


Figure 11 a Strain hardening rate curves for different heat treatment processes and b, c local strain hardening rate curves corresponding to the rate shown in a.

samples can hinder the strain concentration during the tensile process, and this results in a uniform strain distribution and a delay in the fracture. Therefore, PM-BF-RA samples can achieve good strength-plastic matching.

Analysis of impact toughness and hardness

PM-BF-RA samples possess higher hardness than BF-RA samples. This is because of the following two factors: (1) the thickness of bainitic ferrite determines the hardness of the microstructure, and PM-BF-RA samples contain finer bainitic ferrite laths. (2) The small-sized and carbon-rich retained austenite with plastic constraint is beneficial for improving the hardness [51]. The size of the blocky retained austenite in PM-BF-RA samples is much smaller than that in BF-RA samples, and its carbon content is close to that of film austenite in BF-RA samples. These characteristics are beneficial for improving the hardness.

In nanobainite steel, retained austenite with small size and high mechanical stability can alleviate the stress concentration load, reduce the crack propagation rate, and delay crack initiation. These characteristics can improve the toughness [34, 52]. Moreover, larger blocky retained austenite has the opposite effect on impact toughness. Also, PM undergoes self-tempering and discharges carbon into the surrounding untransformed austenite during the below- M_s austempering process, resulting in better toughness of PM. Compared with hard and brittle stress-induced martensite or quenched martensite, PM exhibits excellent coordinated deformation ability, which can share part of the stress between retained austenite and bainitic ferrite interfaces in the impact process [13, 26]. Moreover, the finer bainitic ferrite laths in PM-BF-RA samples provide more interfaces, and this alleviates crack propagation. Therefore, although PM-BF-RA samples have a lower volume fraction of retained austenite, its impact energy is significantly higher.

Conclusions

In this paper, the characteristics of multiphase microstructures in medium carbon bainitic steel and the comprehensive effect of different multiphase

microstructures on mechanical properties were studied. The main conclusions are summarized as follows:

1. Compared with the BF-RA samples, PM-BF-RA samples contain thinner bainitic ferrite with higher dislocation density, and smaller blocky retained austenite with higher carbon content. The introduced pre-formed martensite and low austempering temperature increase the nucleation sites of bainitic ferrite, as well as the strength of undercooled austenite, which refine the size of bainitic ferrite lath.
2. The PM-BF-RA samples exhibit higher strength and hardness. The strengthening model established on the PM-BF-RA microstructural characteristic parameters matches the experimental results well, and the error is only in the range of 1.3–3.8%. The dominant phase in the BF-RA samples is single phase of bainitic ferrite, while that in PM-BF-RA sample is bainitic ferrite and pre-formed martensite. The contribution mechanisms of the yield strength of different phases are different. Grain boundary strengthening contributes most to the strength of bainitic ferrite, while solution strengthening contributes most to the strength of pre-formed martensite and retained austenite.
3. The small-sized retained austenite with high carbon content can produce more effective TRIP effect and improve plasticity in the PM-BF-RA samples. Bainitic ferrite with thin thickness and retained austenite with small size in PM-BF-RA samples can provide more interfaces to delay crack propagation and improve toughness. Medium carbon bainitic steel with PM-BF-RA microstructure achieves excellent combination of strength, plasticity and toughness.

Acknowledgements

This work was funded by the National Natural Science Foundation of China (No. 51471147) and Innovation Ability Promotion Program of Hebei (22567609H).

Authors contribution

XS and TW were involved in conceptualization; YW and GS helped in methodology; XS contributed to formal analysis; XS and YW were involved in investigation; TW helped in resources; XS and DS contributed to data curation; XS and DS were involved in writing—original draft preparation; XS and DS were involved in writing—review and editing; XS and YH helped in visualization; TW contributed to supervision; TW helped in funding support.

Data availability

The raw/processed data required to reproduce these findings cannot be shared at this time as the data also forms part of an ongoing study.

Declarations

Conflict of interest The authors declare that they have no known competing financial interests or personal relationships that could have appeared to influence the work reported in this paper.

References

- [1] Caballero FG, Bhadeshia HKDH (2004) Very strong bainite. *Curr Opin Solid St M* 8(3):251–257
- [2] Haiko O, Kaikkonen P, Somani M, Valtonen K, Kmi J (2020) Characteristics of carbide-free medium-carbon bainitic steels in high-stress abrasive wear conditions. *Wear* 456–457:203386
- [3] Kumar A, Makineni SK, Dutta A, Goulas C, Steenberg M, Petrov RH, Sietsma J (2019) Design of high-strength and damage-resistant carbide-free fine bainitic steels for railway crossing applications. *Mater Sci Eng A* 759:210–223
- [4] Zhao J, Wang TS, Lv B, Zhang FC (2015) Microstructures and mechanical properties of a modified high-C-Cr bearing steel with nano-scaled bainite. *Mater Sci Eng A* 628:327–331
- [5] Ravi AM, Navarro-López A, Sietsma J, Santofimia MJ (2020) Influence of martensite/austenite interfaces on bainite formation in low-alloy steels below M_s . *Acta Mater* 188:1–12
- [6] Lu XH, Yang ZH, Qian DS, Lan J, Hua L (2021) Effect of martensite pre-quenching on bainite transformation kinetics, martensite/bainite duplex microstructures, mechanical properties and retained austenite stability of GCr15 bearing steel. *J Mater Res Technol* 15:2429–2438
- [7] Zhao JL, Lv B, Zhang FC, Yang ZN, Qian LH, Chen C, Long XY (2019) Effects of austempering temperature on bainitic microstructure and mechanical properties of a high-C high-Si steel. *Mater Sci Eng A* 742:179–189
- [8] Baradari S, Boutorabi SMA (2015) Effects of isothermal transformation conditions on the microstructure and hardness values of a high-carbon Al-Si alloyed steel. *Mater Des* 86:603–609
- [9] Jian F, Frankenbach T, Wettlaufer M (2017) Strengthening 42CrMo4 steel by isothermal transformation below martensite start temperature. *Mater Sci Eng A* 683:110–115
- [10] Yang ZN, Liu CB, Zhang CY, Fang QW, Li YG, El-Fallah GMAM, Ooi SW, Zhang FC (2021) Microplasticity behavior of multiphase high-strength nanobainitic steel based on a modified law of mixtures. *Mater Sci Eng A* 825:141848
- [11] Zhao JL, Zhang FC, Lv B, Yang ZN, Chen C, Long XY, Zhao XJ, Chu CH (2019) Inconsistent effects of austempering time within transformation stasis on monotonic and cyclic deformation behaviors of an ultrahigh silicon carbide-free nanobainite steel. *Mater Sci Eng A* 751:80–89
- [12] Long XY, Zhao GC, Zhang FC, Xu S, Yang ZN, Du GJ, Branco R (2020) Evolution of tensile properties with transformation temperature in medium-carbon carbide-free bainitic steel. *Mater Sci Eng A* 775:138964
- [13] Qian LH, Li Z, Wang TL, Li DD, Zhang FC, Meng JY (2022) Roles of pre-formed martensite in below- M_s bainite formation, microstructure, strain partitioning and impact absorption energies of low-carbon bainitic steel. *J Mater Sci Technol* 96:69–84
- [14] Pashangeh S, Somani M, Banadkoukia SSG (2020) Microstructural evolution in a high-silicon medium carbon steel following quenching and isothermal holding above and below the M_s temperature. *J Mater Sci Technol* 9(3):3438–3446
- [15] Garcia-Mateo C, Caballero FG, Bhadeshia HKDH (2005) Mechanical properties of low-temperature bainite. *Mater Sci Forum* 500–501:495–502
- [16] Tan X, Xu Y, Yang X, Wu D (2014) Microstructure-properties relationship in a one-step quenched and partitioned steel. *Mater Sci Eng A* 589:101–111
- [17] Zhao LJ, Qian LH, Zhou Q, Li DD, Wang TL, Jia ZG, Zhang FC, Meng JY (2019) The combining effects of ausforming and below- M_s or above- M_s austempering on the transformation kinetics, microstructure and mechanical properties of low-carbon bainitic steel. *Mater Des* 183:108–123
- [18] Guo H, Feng XY, Zhao AM, Li Q, Ma J (2019) Influence of prior martensite on bainite transformation, microstructures,

- and mechanical properties in ultra-fine bainitic steel. *Materials* 12(3):527
- [19] Navarro-López A, Hidalgo J, Sietsma J, Santofimia MJ (2018) Influence of the prior athermal martensite on the mechanical response of advanced bainitic steel. *Mater Sci Eng A* 735:343–353
- [20] Hasan HS, Peet MJ, Avettand-Fènoël M-N, Bhadeshia HKDH (2014) Effect of tempering upon the tensile properties of a nanostructured bainitic steel. *Mater Sci Eng A* 615:340–347
- [21] Foster D, Paladugu M, Hughes J, Kapousidou M, Barcellini C, Daisenberger D, Jimenez-Melero E (2020) Comparative micromechanics assessment of high-carbon martensite/bainite bearing steel microstructures using in-situ synchrotron X-ray diffraction. *Materialia* 14:100948
- [22] Abbaszadeh P, Kheirandish S, Saghafian H, Goodarzy MH (2017) Effect of austenitizing temperature on mechanical properties of the mixed bainite-martensite microstructure in CrMoV steel. *Mater Res* 21(1):0469
- [23] Garcia-Mateo C, Caballero FG, Sourmail T, Kuntz M, Cornide J, Smanio V, Elvira R (2012) Tensile behaviour of a nanocrystalline bainitic steel containing 3 wt% silicon. *Mater Sci Eng A* 549:185–192
- [24] Zhao JL, Zhao XM, Dong CY, Zhao XY, Kang SX (2018) Effect of bainitic transformation combined with hot forming on the microstructure and mechanical properties of bainite-martensite multiphase steel. *Mater Sci Eng A* 731:102–106
- [25] Avishana B, Khoshkebari SM, Yazdani S (2021) Effect of pre-existing martensite within the microstructure of nano bainitic steel on its mechanical properties. *Mater Chem Phys* 260:124160
- [26] Long XY, Sun DY, Wang K, Zhang FC, Yang ZN, Li YG, Zheng CL (2022) Effect of carbon distribution range in mixed bainite/martensite/retained austenite microstructure on mechanical properties. *J Mater Res Technol* 17:898–912
- [27] De AK, Murdock DC, Mataya MC, Speer JG, Matlock DK (2004) Quantitative measurement of deformation-induced martensite in 304 stainless steel by X-ray diffraction. *Scripta Mater* 50(12):1445–1449
- [28] Williamson GK, Smallman RE III (1956) Dislocation densities in some annealed and cold-worked metals from measurements on the X-ray debye-scherrer spectrum. *Philos Mag* 1(1):34–46
- [29] Germain L, Gey N, Mercier R, Blaineau P, Humbert M (2012) An advanced approach to reconstructing parent orientation maps in the case of approximate orientation relations: Application to steels. *Acta Mater* 60:4551–4562
- [30] Garcia-Mateo C, Caballero FG, Bhadeshia HKDH (2003) Acceleration of Low-temperature Bainite. *ISIJ Int* 43(11):1821–1825
- [31] Koistinen D, Marburger R (1959) A general equation prescribing the extent of the austenite-martensite transformation in pure iron-carbon alloys and plain carbon steels. *Acta Metall* 7:59–60
- [32] Dyson DJ, Holmes B (1970) Effect of alloying additions on the lattice parameter of austenite. *J Iron Steel Inst* 208:469–474
- [33] Rakha K, Beladi H, Timokhina H, Xiong XY, Kabra S, Liss K-D, Hodgson P (2014) On low temperature bainitic transformation characteristics using in-situ neutron diffraction and atom probe tomography. *Mater Sci Eng A* 589:303–309
- [34] Wang XB, Liu CB, Qin YM, Li YG, Yang ZN, Long XY, Wang MM, Zhang FC (2022) Effect of tempering temperature on microstructure and mechanical properties of nanostructured bainitic steel. *Mater Sci Eng A* 832:142357
- [35] Xiong XC, Chen B, Huang MX, Wang JF, Wang L (2013) The effect of morphology on the stability of retained austenite in a quenched and partitioned steel. *Scr Mater* 68:321–324
- [36] M. Peet, H.K.D.H. Bhadeshia, Available online: <https://www.msm.cam.ac.uk/map/steel/tar/mucg83.exe>
- [37] Yoozbashi MN, Yazdani S, Wang TS (2011) Design of a new nanostructured, high-Si bainitic steel with lower cost production. *Mater Des* 32(6):3248–3253
- [38] Kawata H, Hayashi K, Sugiura N, Yoshinaga N, Takahashi M (2010) Effect of martensite in initial structure on bainite transformation. *Mater Sci Forum* 638–642:3307–3312
- [39] Gong W, Tomota Y, Harjo S, Su YH, Aizawa K (2015) Effect of prior martensite on bainite transformation in nanobainite steel. *Acta Mater* 85:243–249
- [40] Toji Y, Matsuda H, Raabe D (2016) Effect of Si on the acceleration of bainite transformation by pre-existing martensite. *Acta Mater* 116:250–262
- [41] Yan JJ, Song H, Dong YP, Quach WM, Yan M (2020) High strength (~2000MPa) or highly ductile (~11%) additively manufactured H13 by tempering at different conditions. *Mater Sci Eng A* 773:138845
- [42] Carretero Olalla V, Bliznuk V, Sanchez N, Thibaux P, Kestens LAI, Petrov RH (2014) Analysis of the strengthening mechanisms in pipeline steels as a function of the hot rolling parameters. *Mater Sci Eng A* 604:46–56
- [43] Kamikawa N, Sato K, Miyamoto G, Murayama M, Sekido N, Tsuzaki K, Furuhashi T (2016) Stress-strain behavior of ferrite and bainite with nano-precipitation in low carbon steels. *Acta Mater* 83:383–396
- [44] Winchell PG, Cohen M (1962) The strength of martensite. *Trans ASM* 55:347
- [45] Langford G, Cohen M (1970) Calculation of cell-size strengthening of wire-drawn iron. *Metall Mater Trans B* 1:1478–1480

- [46] Young CH, Bhadeshia HKDH (1994) Strength of mixtures of bainite and martensite. *Mater Sci Technol* 10:209
- [47] Hutchinson B, Hagström J, Karlsson O, Lindell D, Tornberg M, Lindberg F, Thuvander M (2011) Microstructures and hardness of as-quenched martensites (0.1–0.5%C). *Acta Mater* 59:5845–5858
- [48] Cao J, Yong Q, Liu Q, Sun X (2007) Precipitation of MC phase and precipitation strengthening in hot rolled Nb–Mo and Nb–Ti steels. *J of Mater Sci* 42(24):10080–10084
- [49] Zhou Q, Qian LH, Meng JY, Zhao LJ, Zhang FC (2015) Low-cycle fatigue behavior and microstructural evolution in a low-carbon carbide-free bainitic steel. *Mater Des* 85:487–496
- [50] Navarro-López A, Hidalgo J, Sietsma J, Santofimia MJ (2020) Unravelling the mechanical behaviour of advanced multiphase steels isothermally obtained below M_s . *Mater Des* 188:108484
- [51] Bhadeshia HKDH (2015) *Bainite in steels: theory and practice*, Third Edition. pp 92–94, University of Cambridge
- [52] Gao G, Zhang H, Gui X, Luo P, Tan Z, Bai B (2014) Enhanced ductility and toughness in an ultrahigh-strength Mn-Si-Cr-C steel: the great potential of ultrafine filmy retained austenite. *Acta Mater* 76:425–433

Publisher's Note Springer Nature remains neutral with regard to jurisdictional claims in published maps and institutional affiliations.

Springer Nature or its licensor holds exclusive rights to this article under a publishing agreement with the author(s) or other rightsholder(s); author self-archiving of the accepted manuscript version of this article is solely governed by the terms of such publishing agreement and applicable law.